JunB is required for endothelial cell morphogenesis by regulating core-binding factor β

Alexander H. Licht,[1] Oliver T. Pein,[1] Lore Florin,[1] Bettina Hartenstein,[1] Hendrik Reuter,[2] Bernd Arnold,[3] Peter Lichter,[2] Peter Angel,[1] and Marina Schorpp-Kistner[1]

[1]Division of Signal Transduction and Growth Control, [2]Division of Molecular Genetics, and [3]Division of Molecular Immunology, German Cancer Research Center (Deutsches Krebsforschungszentrum), D-69120 Heidelberg, Germany

The molecular mechanism triggering the organization of endothelial cells (ECs) in multicellular tubules is mechanistically still poorly understood. We demonstrate that cell-autonomous endothelial functions of the AP-1 subunit JunB are required for proper endothelial morphogenesis both in vivo in mouse embryos with endothelial-specific ablation of JunB and in in vitro angiogenesis models. By cDNA microarray analysis, we identified core-binding factor β (CBFβ), which together with the Runx proteins forms the heterodimeric core-binding transcription complex CBF, as a novel JunB target gene. In line with our findings, expression of the CBF target MMP-13 was impaired in JunB-deficient ECs. Reintroduction of CBFβ into JunB-deficient ECs rescued the tube formation defect and MMP-13 expression, indicating an important role for CBFβ in EC morphogenesis.

Introduction

The vascular system is the first functionally developed organ system during ontogeny. The development of blood vessels starts with differentiation of mesodermal precursor cells toward endothelial cells (ECs), hematopoietic cells, and vascular smooth muscle cells. The first vascular plexus in embryos is formed by de novo aggregation of hemangioblasts (vasculogenesis). Thereafter, vessel growth mainly occurs by the sprouting of capillaries from preexisting vessels (angiogenesis; Risau, 1997; Carmeliet, 2000). Endothelial sprouting is a complex process that involves the increase of vascular permeability, vessel wall disassembly, degradation of the basement membrane, migration and proliferation of ECs, and, finally, the formation of a capillary lumen. The newly formed sprouts are subsequently stabilized by formation of cellular junctions, extracellular matrix deposition, and recruitment of perivascular cells (Pepper, 2001; Jain, 2003). Among other proteases, matrix metalloproteinases (MMPs) are required for proteolytic remodeling of the extracellular matrix. Degradation of the EC basement membrane, as well as cleavage of helical interstitial collagens, is rate limiting for endothelial sprouting (Pepper, 2001; Seandel et al., 2001; Davis and Senger, 2005).

Although angiogenic signaling through growth factors like VEGF or basic FGF and their receptors has been studied in great detail, the role of endothelial transcription factors orchestrating the angiogenic response is less well understood. Genetic approaches suggested that transcription factors of the hypoxia-inducible factor, Ets, Gata, Hox, Hey, SCL/Tal, and Smad families are implicated in different stages of vascular development (Oettgen, 2001; Coultas et al., 2005). Recently, an increasing body of evidence associated members of the Activator Protein-1 (AP-1) family of transcription factors either directly or by cooperation with aforementioned factors with angiogenic responses and/or programs (Schorpp-Kistner et al., 1999; Gerald et al., 2004; Zhang et al., 2004). AP-1 consists of homo- or heterodimers of Jun (c-Jun, JunB, and JunD), Fos (c-Fos, FosB, Fra-1, and -2), and ATF (ATF-2, -3, -4, and ATFa) family members (Angel and Karin, 1991; Eferl and Wagner, 2003; Hess et al., 2004). Although different Jun factors have been reported to regulate genes implicated in angiogenesis, like VEGF and MMPs (Schorpp-Kistner et al., 1999; Eferl and Wagner, 2003; Zhang et al., 2004), a direct link between endothelial Jun proteins and angiogenesis has thus far remained questionable. When the different Jun members were deleted in mice, only JunB-deficient embryos displayed vascular abnormalities and died between embryonic day (E)8.5 and E10 because of placental failure (Schorpp-Kistner et al., 1999). Conditional gene targeting

A.H. Licht and O.T. Pein contributed equally to this paper.

Correspondence to M. Schorpp-Kistner: marina.schorpp@dkfz.de

Abbreviations used in this paper: AP-1, activator protein-1; CBF, core-binding factor; ChIP, chromatin immunoprecipitation; CRE, cAMP responsive element; E, embryonic day; EC, endothelial cell; MMP, matrix metalloproteinase; TRE, 12-*O*-tetradecanoylphorbol-13-acetate–responsive element.

The online version of this article contains supplemental material.

The Journal of Cell Biology, Vol. 175, No. 6, December 18, 2006 981–991
http://www.jcb.org/cgi/doi/10.1083/jcb.200605149

provided novel insight into the physiological processes regulated by JunB. Bone development (Hess et al., 2003; Kenner et al., 2004) and adaptive and innate immunity (Hartenstein et al., 2002; Nausch et al., 2006), as well as wound healing and epidermal proliferation (Zenz et al., 2005; Florin et al., 2006), are affected by the loss of JunB. Furthermore, JunB-deficient mice develop a myeloproliferative disease similar to human chronic myeloid leukemia (Passegue et al., 2001).

We investigated the cell-autonomous role of JunB in EC function in vivo and in vitro. EC-specific ablation of JunB resulted in early embryonic lethality, underscoring an essential role for JunB in vessel development in vivo. We found that capillary sprouting of JunB-deficient aortic explants was strongly diminished, underlining the crucial role of JunB as a regulator of angiogenic programs. Isolated ECs lacking JunB expression failed to form capillary-like structures when cultured on Matrigel. Using cDNA microarray analysis, we identified *core-binding factor β* (*CBFβ*) as a novel JunB target gene. Importantly, reintroduction of CBFβ alone rescued the tube formation defect of JunB-deficient ECs, implying a critical role for CBFβ in EC morphogenesis. In line with these findings, expression of the common AP-1 and CBF target metalloproteinase MMP-13 was impaired. Consequently, ECs isolated from MMP-13–deficient mice failed to form capillary-like networks on Matrigel, thus, recapitulating the phenotype of JunB-deficient ECs.

Results

Embryonic lethality caused by loss of JunB expression in ECs

JunB is expressed in ECs during vascular development (Schorpp-Kistner et al., 1999). To investigate the cell-autonomous function of JunB in ECs, we generated mice that lack JunB expression specifically in their ECs. *Tie-2*-Cre transgenic mice were crossed to *junB* −/flox mice to generate a *junB* −/Δ allele in ECs (*junB* $-/\Delta^{EC}$). To better visualize ECs, the mice were crossed to *Tie-2*-lacZ reporter mice. The Cre-mediated deletion of the *junB* locus was detected by PCR analysis (unpublished data). Coexpression of JunB and the EC marker CD31 was confirmed by immunofluorescence staining of control embryos (Fig. 1 B). In contrast, *junB* $-/\Delta^{EC}$ embryos showed no JunB expression in blood vessels, whereas other cell types (e.g., neurons) retained JunB expression. These data confirm the efficient deletion of the floxed allele, specifically in ECs. Embryonic lethality was observed around E10 in *junB* $-/\Delta^{EC}$ mice. The embryos were already severely retarded at E9.5 compared with controls (Fig. 1 A). Embryos had not yet turned and displayed enlarged pericardial sacs. At E10.5, control mice developed a highly organized vascular tree in the head region, whereas *junB* $-/\Delta^{EC}$ embryos showed a disorganized vasculature with aberrantly branching and dilated vessels (Fig. 1 A). Additionally, the yolk

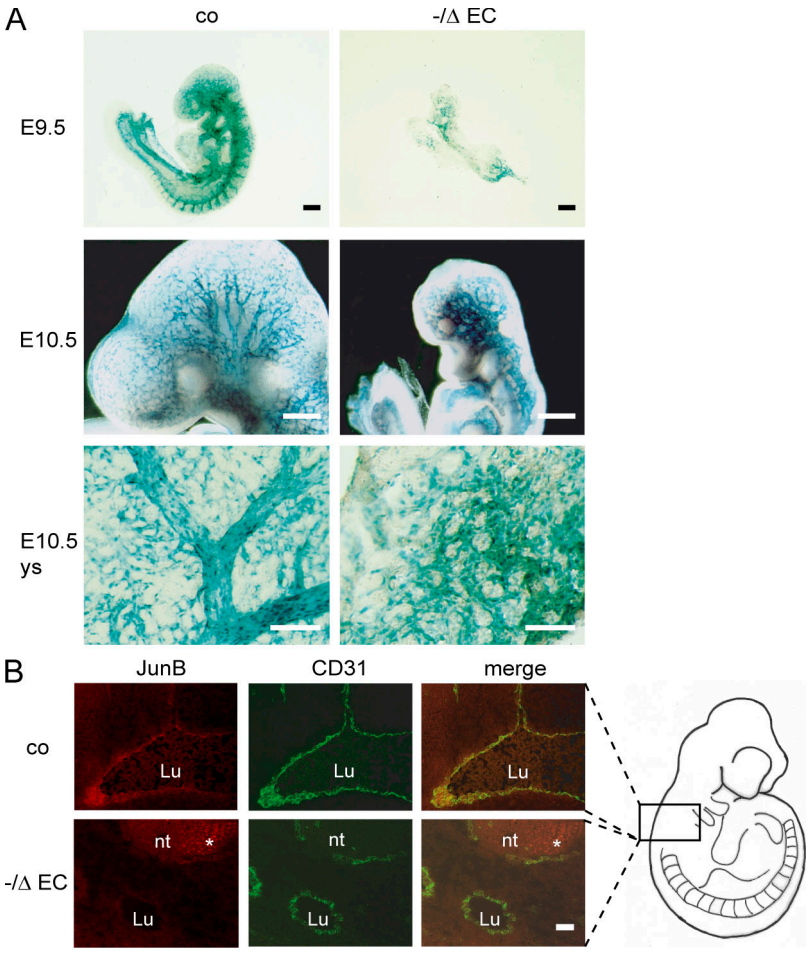

Figure 1. **Endothelium-specific deletion of *junB* disrupts vascular development.** *junB* $-/\Delta^{EC}$ embryos were generated by mating *Tie-2*-Cre/*junB* +/− and *junB* flox mice. (A) All embryos carried a *Tie-2*-lacZ transgene to visualize ECs by LacZ activity. Control embryos developed a normal vascular system, whereas *junB* $-/\Delta^{EC}$ embryos were retarded at E9.5, had an enlarged pericardium, and showed a disorganized vasculature. At E10.5, when control embryos had developed a vascular tree in the cephalic region, *junB* $-/\Delta^{EC}$ embryos showed hardly any capillary sprouting and dilated vessels. Highly branched vessel structures were formed in yolk sacs (ys) of control embryos at E10.5, whereas yolk sacs of *junB* $-/\Delta^{EC}$ embryos showed only a primitive vascular plexus. (B) Colocalization of JunB and CD31 was observed by immunofluorescence staining. Control embryos expressed JunB in ECs, whereas in *junB* $-/\Delta^{EC}$ embryos JunB was expressed in neurons (asterisk), but was absent from CD31-positive blood vessels. (right) Schematic view of an embryo is given to indicate analyzed area (boxed region). Lu, lumen; nt, neural tube. Bars: (A) 250 μm; (B) 100 μm.

sacs of *junB* $-/\Delta^{EC}$ embryos showed marked defects in vascular remodeling, as vessels formed only a primitive vascular plexus. In contrast, a hierarchically organized vessel structure developed in control mice (Fig. 1 A). Interestingly, this phenotype closely resembled the vascular defects observed in the embryo proper of the complete *junB* knockout mice (Schorpp-Kistner et al., 1999). However, vascularization of the placenta was not impaired in *junB* $-/\Delta^{EC}$ mice (Fig. S1, available at http://www.jcb.org/cgi/content/full/jcb.200605149). These data define an important role for JunB in the endothelial lineage in vivo.

Capillary sprouting of aortic explants is severely impaired in JunB-deficient mice

Because of the early embryonic death, it was difficult to investigate altered EC function in *junB* $-/\Delta^{EC}$ mice. Therefore, we used a second transgenic mouse model with conditional inactivation of JunB. In *Collagen1α2*-Cre/*junB* $-/\Delta$ mice (*junB* $-/\Delta^{Coll}$), efficient recombination of the *junB* locus occurred in many cell types, as reported previously (Florin et al., 2006). In contrast to completely JunB-deficient mice, these animals were viable (Florin et al., 2006) because of the fact that the deletion of *junB* occurred at a later stage of embryonic development (around E14; unpublished data). Analysis of genomic DNA revealed complete *junB* deletion in aortic tissue and isolated primary ECs of *junB* $-/\Delta^{Coll}$ mice (Fig. 2 A). To prove loss of JunB expression on protein level, primary ECs were isolated from these mice. Expression of endothelial marker proteins was confirmed by FACS analysis and immunofluorescence staining for CD31, endoglin (CD105), VEGFR-2, or VE-cadherin (Fig. 2 B and not depicted), demonstrating the isolation of a 94–98% pure population of ECs. Immunoblotting revealed that the JunB protein was indeed undetectable in *junB* $-/\Delta^{Coll}$ ECs, whereas it was expressed in control ECs (Fig. 2 C).

To investigate whether *junB* $-/\Delta^{Coll}$ mice have a defect in blood vessel growth, mouse aortic ring assays were performed with explanted tissue of control or *junB* $-/\Delta^{Coll}$ aortae (Fig. 2 D). Within 7 d of explant culture, strong outgrowth of capillary sprouts from the aortic rings was observed in control (Fig. 2 D) or *Tie-2*-lacZ reporter mice. Staining for LacZ activity or immunofluorescence staining for CD31 confirmed that these sprouts originate from ECs and that they form a vessel lumen (Fig. S2, A–E, available at http://www.jcb.org/cgi/content/full/jcb.200605149). In contrast, *junB* $-/\Delta^{Coll}$ rings showed nearly no capillary outgrowth (Fig. 2 D). To exclude that the effect is solely caused by paracrine VEGF acting on ECs, aortic ring assays were performed in the presence of exogenously added recombinant VEGF. In control aortae, the addition of VEGF to the medium did not further increase the already strong sprouting activity (Fig. 2 E), indicating that the VEGF levels in the medium are already in a saturation range. In *junB* $-/\Delta^{Coll}$ explants, additional VEGF had no effect on sprout formation (Fig. 2 E). Thus, VEGF is not the limiting factor for sprouting in this system, and JunB most likely induces capillary growth via other mechanisms.

Impaired capillary-like tube formation of JunB-deficient ECs

The capability of primary ECs to form tube-like structures was investigated upon cultivation on Matrigel (Fig. 3 A). Control ECs formed capillary-like structures that connected to anastomosing networks within 18 h in culture. In sharp contrast, *junB* $-/\Delta^{Coll}$ ECs largely failed to generate tubes, but instead formed cellular aggregates, even if cultured for longer time periods. Like in the aortic ring assay, addition of recombinant VEGF did not rescue the tube formation defect (unpublished data). Our finding was supported by the use of a second model involving JunB-deficient transformed ECs, so-called endothelioma (END) cells that provide a model for activated embryonic endothelium (Reiss et al., 1998). Control END cells formed tubelike structures and networks of EC cords very rapidly (within 6 h) on Matrigel (Fig. 3 A). As observed for *junB* $-/\Delta^{Coll}$ ECs, cord formation of JunB-deficient END cells was drastically decreased (13% of the control cells), which was quantified by counting interendothelial spaces (Fig. 3 C). A similar phenotype was observed with END cells derived from *junB* flox/flox mice, in which the floxed allele was deleted by transduction of a retroviral Cre expression vector (*junB* Δ/Δ; Fig. 3 A, bottom). The floxed allele was efficiently deleted (~90%), as revealed by FACS analysis for IRES-eGFP expression (unpublished data) and PCR amplification of the recombined locus (Fig. 3 B).

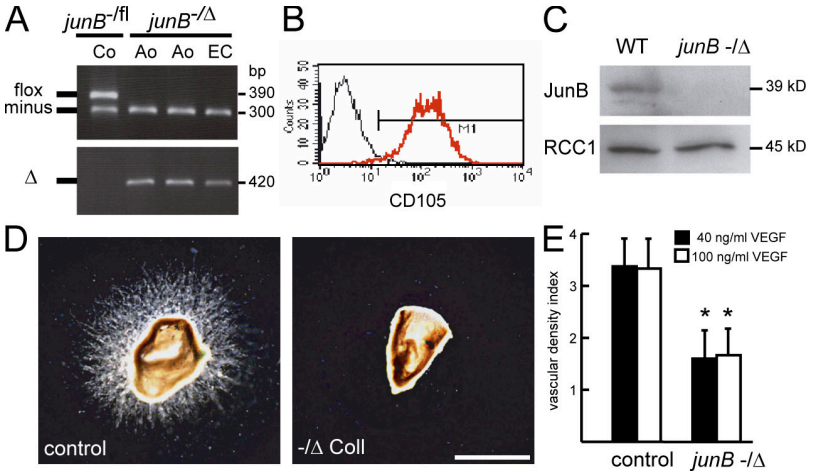

Figure 2. **Reduced sprouting of JunB-deficient aortic explants.** (A) Complete deletion of the *junB* locus was verified by PCR in aortae (Ao) or primary ECs of *junB* $-/\Delta^{coll}$ mice. (B) FACS analysis for the endothelial marker CD105 (red line) confirmed the isolation of a >94% (M1) pure population of ECs. (C) Immunoblotting revealed complete loss of JunB in nuclear extracts of *junB* $-/\Delta^{coll}$ ECs. (D) Aortic ring assay was performed using control or *junB* $-/\Delta^{coll}$ mice. Bar, 770 µm. (E) To enhance vascular density, the aortic explants were cultured in medium containing 40 or 100 ng/ml recombinant VEGF. Under both conditions, vascular density was significantly lower in *junB* $-/\Delta^{coll}$ aortae compared with the controls. Error bars indicate the SD. *, $P < 0.05$.

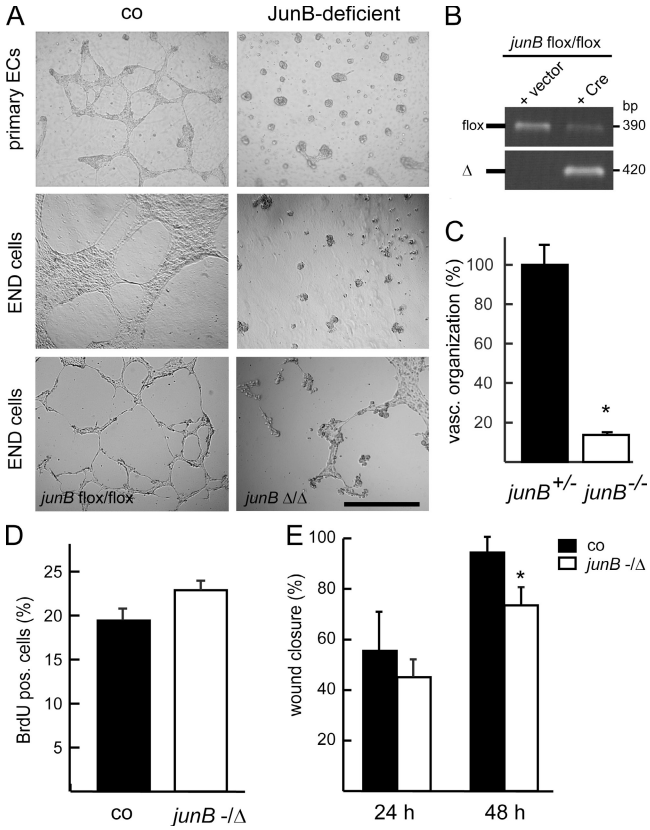

Figure 3. **Capillary-like tube formation is impaired in JunB-deficient ECs.** (A) Control primary ECs and END cells formed capillary-like networks when cultured on Matrigel for 18 or 6 h, respectively, whereas JunB-deficient cells failed to form capillary-like structures under the same conditions. A similar phenotype was observed for *junB* Δ/Δ END cells in which the *junB* locus was recombined by retroviral Cre transduction in vitro. Bar, 670 μm. (B) PCR analysis revealed that the *junB* floxed allele was efficiently deleted in END cells transduced with a retroviral Cre expression vector, but not in cells transduced with empty vector. (C) The degree of vascular organization of END cells was quantified by counting interendothelial spaces. JunB-deficient cells only achieved 13% of the network organization compared with control cells. (D) Proliferation was assessed by BrdU incorporation, which revealed no differences between control and *junB* −/Δ ECs. (E) EC monolayers were scratched and wound closure was monitored after 24 and 48 h. JunB-deficient cells showed slightly delayed wound closure after 48 h. Error bars indicate the SD. * $P < 0.05$.

Defective tube formation could be caused by a failure in proliferation; thus, the proliferation rate of control and *junB* $-/\Delta^{Coll}$ ECs was determined by BrdU incorporation and subsequent FACS analysis, which revealed no considerable difference (Fig. 3 D). Lateral migration was investigated by scratching EC monolayers and by monitoring wound closure after 24 and 48 h. A slight delay in wound closure was observed in JunB-deficient cells after 48 h (Fig. 3 E); however, these small differences in migration alone cannot account for the severe defects in tube formation (Fig. 3 A). The expression levels of genes typically involved in angiogenesis were analyzed by RT-PCR. No differences in expression of *angiopoietin-1* and *-2* or their receptors *tie-1* and *-2* were observed. Decreased *VEGF* levels were found, but the main signaling receptor, *VEGFR-2*, was unaffected. In addition, similar levels of the AP-1 family members c-Jun, c-Fos, and ATF-2 were detected in control and JunB-deficient ECs (unpublished data). Collectively, analysis of proliferation, migration, and expression of known angiogenic candidate genes did not reveal first signs for a mechanism that could explain the phenotype of JunB-deficient cells. Therefore, a systematic approach was chosen to compare the gene expression profiles of JunB-deficient and control cells.

cDNA microarray analysis identifies novel JunB target genes

To search for target genes affected by the loss of JunB in the endothelium, large-scale comparative gene expression analysis was performed using cDNA microarray technology. JunB expression is highly up-regulated by hypoxia (Fig. 4 B); thus, a combinatorial analysis of gene expression was performed in control and JunB-deficient ECs cultured under normoxia or hypoxia. Under hypoxic conditions, 729 genes were up-regulated in control cells, whereas the expression of 956 genes was repressed. However, by comparing the expression profile of control with JunB-deficient cells under hypoxic conditions, only 23 genes were up-regulated and 16 genes were repressed in a strictly JunB-dependent manner. The newly identified JunB-dependent genes (Table I) included transcription factors (*CBFβ*, *LBP-1a*, *Creb3l2*, *Pou6f1*, *Klf16*, and *FoxJ2*), factors involved in protein synthesis (*Farsla*, *Aars*, and *Eif3s10*), genes involved in intracellular trafficking (*Tram1*, *Kif5b*, and *Myo1D*), genes involved in cytoskeletal architecture (*Nestin*, *Rhophilin-2*, and *Tbcd*), and genes regulating apoptosis (*Diablo* and *Nix*) and metabolism (*Acsl4*, *Aldh1b1*, *Fdft1*, and *Tgm2*).

CBFβ is induced by hypoxia in a JunB-dependent manner

Of the newly identified JunB target genes, our attention was attracted by CBFβ. AP-1 and CBF factors physically interact in a transcriptional complex and transactivate common target genes (Selvamurugan et al., 1998; Hess et al., 2001). CBFβ is the common partner of the Runt-related transcription factors (Runx). Real-time RT-PCR analysis confirmed the results from the microarray analysis, showing a 3.3-fold induction of CBFβ under hypoxia, which was lost in *junB* −/− END cells, as well as in Cre-transduced *junB* Δ/Δ cells (Fig. 4 A and not depicted). Induction of CBFβ correlated with that of JunB by hypoxia in END cells (Fig. 4 B). To confirm that CBFβ is a JunB target in vivo, bone marrow cells were isolated from control and JunB-deficient mice. Indeed, CBFβ expression was considerably reduced (by 60%) in the absence of JunB, as determined by real-time RT-PCR and Western blot analysis (Fig. 4 C). Moreover, immunofluorescence staining was performed on embryo sections of *junB* $-/\Delta^{EC}$ and control embryos. CBFβ expression colocalized with CD31-positive vessels in control embryos, whereas no CBFβ signal was detected in vessels of *junB* $-/\Delta^{EC}$ embryos (Fig. 4 D). To investigate whether CBFβ is a direct JunB target, the murine *CBFβ* promoter region was cloned and different fragments were fused to a luciferase reporter gene. Promoter analysis revealed three potential AP-1 binding sites (12-*O*-tetradecanoylphorbol-13-acetate–responsive elements [TREs]) in the distal promoter region (nt −1,496 to −1,061) and one TRE and two cAMP-responsive elements (CREs) in

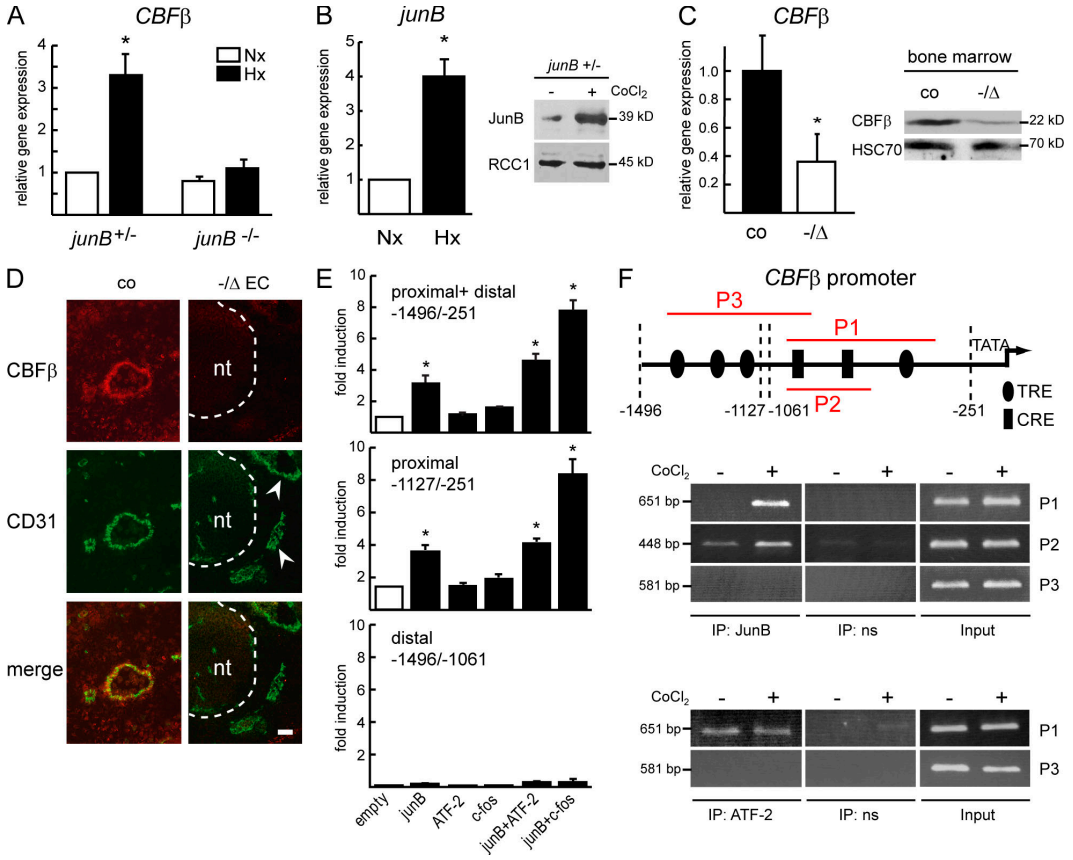

Figure 4. **CBFβ expression is regulated by JunB.** (A) Real-time RT-PCR analysis revealed induction of CBFβ after 16 h hypoxia in control END cells. In JunB-deficient END cells, CBFβ expression was not inducible by hypoxia. (B) Under the same conditions, JunB expression was up-regulated fourfold. Western blot analysis confirmed induction of JunB on protein level after $CoCl_2$ treatment. (C) Real-time RT-PCR and Western blot analysis revealed strongly diminished CBFβ expression in bone marrow cells of *junB* $-/\Delta^{coll}$ mice compared with control mice. (D) Immunofluorescence staining for CBFβ was performed on sections of control or *junB* $-/\Delta^{EC}$ embryos. CBFβ expression colocalized with CD31-positive vessels in control embryos, whereas no signal was detected in *junB* $-/\Delta^{EC}$ embryos. Bar, 100 μm. nt, neural tube. Arrowheads indicate blood vessels. Adjacent sections of embryo shown in Fig.1 B were used. (E) Fragments of the CBFβ promoter (−1496/−251, −1127/−251, and −1496/−1061) fused to a luciferase reporter gene were cotransfected with *junB*, *ATF-2*, or *c-fos* in F9 carcinoma cells. The proximal fragment harboring only the proximal CRE and TRE elements (−1127/−251) shows a similar activity as the reporter with both distal and proximal CRE and TRE sites (−1496/−251). Expression of JunB induced the promoter, whereas ATF-2 or c-Fos had no effect. JunB in combination with either ATF-2 or c-Fos led to a strong transactivation of these two CBFβ promoter fragments, whereas promoter activity of the reporter containing solely the distal TRE elements (−1496/−1061) was hardly detectable. (F) ChIP analysis of the CBFβ promoter was performed using antibodies for JunB or ATF-2. Specific primer sets were used to discriminate promoter elements (P1, P2, and P3). JunB binding to the CBFβ promoter was detected at the proximal CRE and TRE (P1 and P2) and was strongly enhanced in ECs treated with 200 μM $CoCl_2$ for 4 h. Binding of ATF-2 also occurred at the proximal promoter region (P1), whereas no binding of JunB or ATF-2 was found at the distal TRE sites (P3). Error bars indicate the SD. *, $P < 0.05$.

the proximal promoter region (nt −1,127 to −251; Fig. 4 F, top). Coexpression of either the complete or proximal reporter constructs (nt −1,496 to −251 or −1,127 to −251) with a JunB expression vector in F9 teratocarcinoma cells already increased promoter activity by threefold (Fig. 4 E, top). Coexpression of JunB with the dimerization partners ATF-2 or c-Fos further increased CBFβ promoter activity four- or eightfold induction, respectively, whereas expression of ATF-2 or c-Fos alone had no effect (Fig. 4 E, top). The region containing the three distal TREs alone (nt −1,496 to −1,061) showed hardly any activity in this assay (Fig. 4 E, bottom); therefore, we hypothesized that JunB binding to the CBFβ promoter should take place at the proximal CREs and TRE. To finally prove the physical interaction of JunB with the CBFβ promoter, chromatin immunoprecipitation (ChIP) analysis was performed in ECs in the absence or presence of $CoCl_2$. Primers were designed to amplify specific regions of the CBFβ promoter (P1, P2, and P3) that contain the TRE and CREs for potential binding of JunB. We found JunB binding at the proximal CREs and TRE (Fig. 4 F, P1 and P2). This binding was strongly enhanced in $CoCl_2$-treated cells. In contrast, no interaction was observed at the three distal TREs (P3), confirming the data of the luciferase reporter assay (Fig. 4 E). To find the dimerization partner of JunB regulating CBFβ expression, ChIP analysis was performed using antibodies against ATF-2, c-Fos, and Fra-1 that are expressed in ECs. We only detected a constitutive interaction of ATF-2 with the *CBFβ* promoter in uninduced and $CoCl_2$-treated ECs (Fig. 4 F, bottom). The binding occurred at the proximal CREs and TRE (P1), in the same region where JunB binding was detected. No ATF-2 binding was found at the three distal TREs. We detected no interaction of c-Fos or Fra-1 with the *CBFβ* promoter (unpublished data). These data

Table I. **Genes regulated by JunB and hypoxia in ECs**

Gene	Gene name	Unigene No.	JunB	Hx	Function
Mospd1	motile sperm domain containing 1	Mm.28236	6.5	2.9	Cytoskeleton
Cbfb	core binding factor beta	Mm.2018	6.5	2.0	Transcription
Cnot6l	CCR4-NOT transcription compl. subunit 6-like	Mm.28374	6.1	2.6	Transcription
Wdr26	WD repeat domain 26	Mm.289082	4.6	4.1	Signaling
Acsl4	acyl-CoA synthetase long chain family 4	Mm.143689	4.2	3.1	Metabolism
Rbmxrt	RNA binding motif protein, X chromosome	Mm.24718	3.6	5.0	Apoptosis
D530031C13Rik	RIKEN cDNA D530031C13 gene	Mm.390454	3.5	3.9	unknown
Ubp1 (LBP-1a)	upstream binding protein 1	Mm.28052	3.5	2.6	Transcription
Tpt1	tumor protein translationally controlled 1	Mm.296922	3.3	3.2	Signaling
Eif3s10	eukar. translation initiation factor 3, subunit 10	Mm.2238	3.2	2.3	Translation
Ncald	neurocalcin delta	Mm.283370	2.9	4.6	Signaling
Creb3l2	CRE-binding protein 3-like 2	Mm.169929	2.9	4.2	Transcription
Top2b	topoisomerase II beta	Mm.130362	2.9	2.3	Transcription
Phf17	PHD finger protein 17	Mm.286285	2.8	14.0	Transcription
Rhpn2	rhophilin-2	Mm.286600	2.5	2.9	Cytoskeleton
Nes	nestin	Mm.331129	2.5	2.5	Cytoskeleton
Scmh1	sex comb on midleg homologue 1	Mm.208924	2.4	3.8	Differentiation
Tram1	translocating chain-assoc. membrane protein 1	Mm.28765	2.4	2.1	Transport
AI848100	expressed sequence AI848100	Mm.170002	2.4	3.2	unknown
Arid2	AT rich interactive domain 2	Mm.17166	2.3	2.3	Transcription
Bnip3l (Nix)	BCL2/adenovirus E1B interacting protein 3-like	Mm.29820	2.2	2.4	Apoptosis
Kif5b	kinesin family member 5B	Mm.223744	2.2	4.5	Transport
Btbd1	BTB domain containing 1	Mm.71103	2.1	3.7	Differentiation
Tbcd	tubulin-specific chaperone d	Mm.23686	−11.2	−2.2	Cytoskeleton
2810428I15Rik	RIKEN cDNA 2810428I15 gene	Mm.28242	−7.7	−3.0	unknown
Diablo	diablo homologue (smac)	Mm.46716	−6.1	−2.5	Apoptosis
Myo 1D	myosin 1 D	Mm.151948	−5.9	−2.6	Transport
Pou6f1	POU domain, class 6, transcription factor 1	Mm.28825	−5.3	−4.0	Transcription
Aldh1b1	aldehyde dehydrogenase 1 family member B1	Mm.331583	−4.5	−29.8	Metabolism
Klf16	kruppel-like factor 16	Mm.41513	−4.4	−3.3	Transcription
3200001K10Rik	RIKEN cDNA 3200001K10 gene	Mm.304075	−4.2	−2.5	unknown
FoxJ2	forkhead box J2	Mm.87142	−3.9	−4.7	Transcription
2900070E19Rik	RIKEN cDNA 2900070E19 gene	Mm.29128	−3.0	−2.2	unknown
Tgm2	transglutaminase 2, c polypeptide	Mm.330731	−3.0	−2.4	Metabolism
Fdft1	farnesyl diphosphate farnesyl transferase 1	Mm.343538	−2.8	−2.8	Metabolism
Farsla	phenylalanine-tRNA synthetase-like, alpha subunit	Mm.292517	−2.6	−2.1	Translation
6720457D02Rik	RIKEN cDNA 6720457D02 gene	Mm.102840	−2.3	−7.4	unknown
Aars	alanyl-tRNA synthetase	Mm.24174	−2.1	−4.0	Translation
Gspt1	G1 to S phase transition 1	Mm.325827	−2.1	−2.8	Translation

Control and JunB-deficient END cells were kept under normoxic or hypoxic conditions for 16 h, and total RNA was isolated and subjected to microarray analysis. The table lists identified genes differentially regulated by JunB and hypoxia. JunB, fold induction of genes in control versus JunB-deficient END cells; Hx, fold induction of genes kept under hypoxia (1.5% O_2) versus normoxia. All genes listed from Tbcd downward are repressed genes.

strongly suggest that either a JunB–JunB homodimer or a JunB–ATF-2 heterodimer regulates CBFβ expression in ECs in vivo.

CBFβ expression in JunB-deficient ECs rescues tube formation defects

To determine whether CBFβ is functionally implicated in the tube-forming process of ECs, we attempted to rescue the phenotype. By retroviral gene transfer CBFβ, JunB, or empty control vector (Fig. S3 A, available at http://www.jcb.org/cgi/content/full/jcb.200605149) were reintroduced into JunB-deficient END cells. After culture in selective medium, >96% of the cells integrated the retroviral vector into their genome, as determined by FACS analysis for the coexpressed IRES-GFP reporter (Fig. S3 B). Immunoblotting confirmed strong expression of CBFβ or JunB in transduced cells (Fig. S3 C). As expected, JunB-deficient END cells transduced with empty vector did not form capillary-like structures when cultured on Matrigel (Fig. 5 A). Tube formation was efficiently rescued by reexpression of JunB in END cells (Fig. 5 A). Most notably, CBFβ expression also rescued tube formation in JunB-deficient cells (Fig. 5 A). To quantify vascular organization in these experiments, the interendothelial spaces were counted, which revealed a significant difference between the END cells transduced with empty vector and those transduced with CBFβ or JunB, respectively (Fig. 5 B). These data underscore a functional implication of CBFβ in the morphogenic process downstream of JunB.

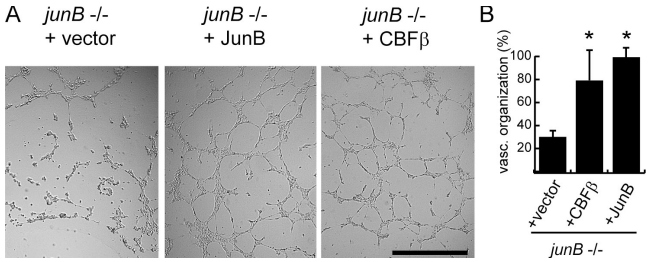

Figure 5. **Reexpression of JunB or CBFβ in JunB-deficient ECs rescues the tube formation defect.** (A) JunB-deficient END cells were transduced with retrovirus containing empty vector, JunB, or CBFβ expression vectors. Capillary-like tube formation on Matrigel was restored by JunB or CBFβ expression, but not by the vector control. Bar, 590 μm. (B) Quantification of the degree of vascular organization yields only 30% for cells transduced with empty vector, but 80% for cells reexpressing CBFβ when compared with JunB-transduced cells (100%). Error bars indicate the SD. *, $P < 0.05$.

Reduced collagenase activity and expression in JunB-deficient ECs

To mechanistically explain the observed defects in sprouting and tube formation of JunB-deficient cells, we studied the invasive capacity of control and JunB-deficient ECs. The ECs were plated on type I collagen gel, and after 10–14 d control cells changed from polygonal to spindlelike morphology and invaded the gel underlying the monolayer. By focusing through the optical planes, cells underneath the monolayer were identified that displayed long cellular protrusions and filopodia, indicating an invasive/angiogenic phenotype (Fig. 6 A). In contrast, JunB-deficient cells formed a monolayer on top of the collagen, but failed to invade deeper into the gel (Fig. 6 A). To investigate the molecular basis of impaired invasion, supernatants of control and *junB* $-/\Delta^{Coll}$ ECs were analyzed for collagenolytic activity. In this assay, native helical collagen served as a substrate, which is cleaved only by MMP-8, -13, and -14. Supernatant of JunB-deficient ECs revealed a 40% decrease in overall collagenase activity (Fig. 6 B), suggesting that reduced collagenase activity accounts for the impaired EC sprouting. RT-PCR analysis revealed strongly reduced expression of not only *MMP-13* but also *MMP-2*, a known JunB target gene (Bergman et al., 2003), in JunB-deficient ECs in comparison to control cells. In contrast, *MMP-9* and *-14* mRNA levels were not affected (Fig. 6 C), whereas *MMP-8* expression was not detectable in cells of both genotypes (unpublished data). The reduced expression of *MMP-2* and *-13* was confirmed by real-time RT-PCR analysis (Fig. 6 D). MMP-13 represents a well-documented common target of AP-1 and CBF transcription factors that can physically interact and cooperate in the transactivation of MMP-13 in osteoblastic cells (Selvamurugan et al., 1998; Hess et al., 2001). We were able to confirm these findings in ECs (Fig. S4, available at http://www.jcb.org/cgi/content/full/jcb.200605149).

The AP-1/CBF target gene *MMP-13* is required for tube formation

To unequivocally determine the function of MMP-13 in this process, primary ECs were isolated from *mmp-13* $-/-$ mice (Stickens et al., 2004; Hartenstein et al., 2006) and applied in a

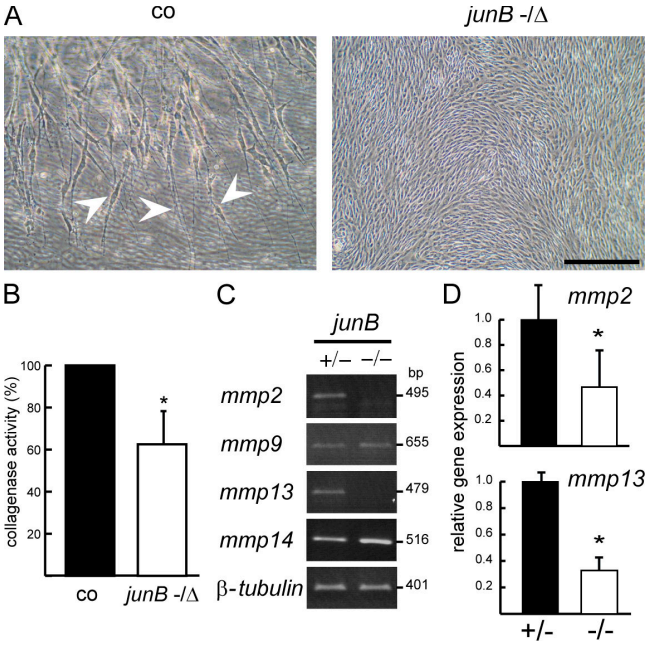

Figure 6. **Impaired invasive capacity of JunB-deficient ECs caused by reduced MMP-13 expression.** (A) Control ECs seeded on collagen gel changed their morphology and invaded the gel. Note the elongated cells extending filopodia (arrowheads). JunB-deficient cells formed a confluent monolayer on top of the collagen gel, but did not invade the gel. Bar, 230 μm. (B) Collagenase activity was determined in the supernatant of ECs. JunB-deficient ECs only showed 60% collagenolytic activity of control cells. (C) RT-PCR analysis revealed expression of MMP-2 and -13 is reduced in JunB-deficient END cells. (D) Real-time RT-PCR confirmed a 50 and 70% down-regulation of MMP-2 or -13, respectively. Error bars indicate the SD. *, $P < 0.05$.

tube formation assay. Indeed, MMP-13–deficient ECs largely failed to form capillary-like networks on Matrigel (14% compared with control cells), confirming an essential role of MMP-13 in tube formation in our model system (Fig. 7, A and B). Finally, we investigated MMP-13 expression in JunB-deficient END cells transduced with CBFβ. Although *junB* $-/-$ END cells transduced with empty vector showed no MMP-13 expression, introduction of CBFβ strongly up-regulated MMP-13 expression (Fig. 7 C). Together, these findings suggest that the defects in tube formation and sprouting observed in JunB-deficient ECs are a consequence of impaired CBFβ expression, resulting in reduced expression of proteases.

Discussion

Previously, we have reported critical functions for JunB in controlling cytokine-regulated mesenchymal–epidermal interactions in skin by regulating keratinocyte proliferation and differentiation in both a paracrine and autocrine manner (Florin et al., 2004b, 2006). Very recently, we could demonstrate an essential role for JunB in basal and hypoxia-mediated VEGF expression and tumor angiogenesis, implying a paracrine mechanism for fibroblast or tumor cell–derived VEGF acting on the endothelium (unpublished data). As JunB is also highly expressed in ECs, in this study we specifically addressed the EC-intrinsic requirement of JunB and JunB-dependent genetic

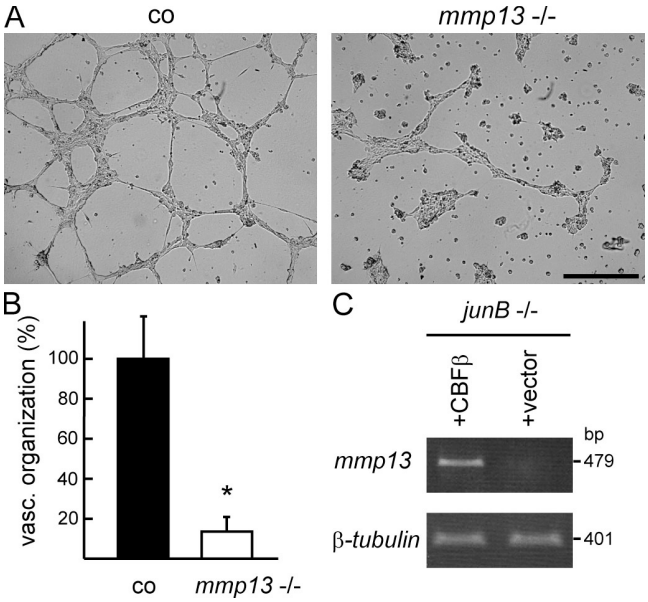

Figure 7. **Loss of MMP-13 in ECs causes failure in tube formation.** (A) Although control ECs formed highly organized networks on Matrigel, MMP-13–deficient ECs displayed a severely impaired capillary-like network formation capability. Bar, 500 μm. (B) Quantification revealed 15% of vascular organization in *mmp-13* −/− ECs, compared with 100% of control cells. (C) Reexpression of CBFβ in JunB-deficient END cells up-regulates MMP-13 expression, whereas the vector control had no effect on MMP-13 expression. Error bars indicate the SD. *, $P < 0.05$.

programs. Indeed, JunB deletion in the endothelial lineage using *Tie-2*-Cre mice resulted in severe vascularization defects in the yolk sac and embryo proper and early embryonic death, suggesting an EC-intrinsic role for JunB. Accordingly, sprout formation of JunB-deficient aortic explants and capability of primary ECs lacking JunB to form capillary-like cords when cultivated on Matrigel was strongly impaired, even in the presence of excessive recombinant VEGF, excluding that limiting VEGF levels account for this phenotype.

In the search for JunB-dependent target genes implicated in EC morphogenesis, we focused on genes differentially expressed in JunB-deficient ECs kept under normoxic or hypoxic conditions compared with control cells to mimic a physiological condition for angiogenesis induction. Applying stringent criteria for expression profiling, 23 up- and 16 down-regulated genes were identified to be dependent on JunB and hypoxia. These genes can functionally be grouped in cytoskeletal components, transcription factors, translational factors, and genes implicated in apoptosis, cellular trafficking, or metabolism.

For example, the group of cytoskeletal genes includes *nestin*, which is an intermediate filament protein that is highly expressed in neuronal stem cells, but also in activated ECs. As *nestin* expression is down-regulated in quiescent ECs, it was recently designated as a specific marker for angiogenic ECs and probably a modulator of cytoskeletal dynamics in activated ECs (Mokry et al., 2004). A second cytoskeletal gene found in our screen is *rhophilin-2*, which encodes a Rho-GTPase–binding protein that modulates Rho activity, and thereby influences rearrangement of the actin cytoskeleton (Peck et al., 2002). Previously, it has been shown that Rho-mediated actin organization is essential for cord formation of angiogenic ECs (Hoang et al., 2004; Liu and Senger, 2004). A second group of JunB target genes is comprised of transcriptional regulators, such as *LBP-1a*, which is a mammalian homologue of the *grainyhead* transcription factor family originally found in *Drosophila melanogaster* and implicated in BMP-4 signaling. Interestingly, LBP-1a–deficient mice display a phenotype very similar to that of JunB knockout mice, as the embryos die at E10 and have severe defects in the vascularization of placenta and yolk sac (Parekh et al., 2004). In summary, the physiological features of these identified target genes imply that JunB is required for the transition from quiescent to angiogenic endothelium.

Yet, we concentrated our analysis on another transcriptional regulator found among the JunB-dependent genes, namely the *CBFβ*, which is the common heterodimerization partner of the Runx comprising the three α-subunits Runx-1 (CBFα-2 and AML-1), -2 (CBFα-1), and -3 (CBFα-3). The Runx–CBFβ dimer binds to a specific DNA sequence and, depending on the recruitment of coactivators or co-repressors, activates or suppresses the transcription of target genes, respectively (Blyth et al., 2005).

Inactivation of the *runx* genes in mice revealed essential functions in definitive hematopoiesis (Runx-1), in bone formation (Runx-2), or in epithelial and neuronal development (Runx-3). Runx-1–deficient embryos had a lower number of small capillaries in the hindbrain; moreover, vessels in the hindbrain, pericardium, and yolk sac showed less branching (Takakura et al., 2000).

Deletion of the CBFβ subunit disrupted normal hematopoiesis and caused embryonic lethality between E12.5 and E13.5. Transgenic CBFβ expression in the hematopoietic system rescued embryonic lethality and revealed impaired bone formation in CBFβ-deficient mice (Speck and Gilliland, 2002; Blyth et al., 2005). Hemorrhages were observed in the cephalic and lumbar region of CBFβ-deficient embryos starting at E10.5. This was associated with perivascular edema and cell death in areas of actively growing capillaries. It was hypothesized that CBFβ may play a role in certain aspects of vessel development, although this was not tested directly (Wang et al., 1996). Moreover, Runx-1 or CBFβ are frequent targets of chromosomal translocation in humans, which account for 25% of adult acute myeloid leukemia. In *junB* $-/\Delta^{Coll}$ mice, CBFβ expression was decreased in bone marrow, which is the major site of endogenous CBFβ expression in vivo. Interestingly, phenotypes of CBFβ- and JunB-deficient mice exhibit striking similarities. Mice with reduced JunB expression develop a leukemia-like disease (Passegue et al., 2001) and have defects in bone formation (Hess et al., 2003; Kenner et al., 2004), providing further physiological evidence for a role of JunB in regulating CBFβ expression.

Our data point to an additional function of CBFβ in the hypoxia-response of ECs. ChIP analysis revealed that *CBFβ* is a direct target gene of JunB in ECs. We demonstrate that CBFβ is functionally important for EC morphogenesis, as reexpression of CBFβ in JunB-deficient ECs rescued tube formation on Matrigel. CBFβ, Runx-1, and -2 expression was reported in ECs (Namba et al., 2000; Sun et al., 2001; Iwatsuki et al., 2005).

In line with our findings, a function of CBFβ in ECs has been proposed previously, as overexpression of a dominant-negative mutant of CBFβ inhibited EC tube formation in type I collagen gels (Namba et al., 2000). Similarly, loss of Runx-1, or a truncated Runx-2 protein, perturbs tube formation on Matrigel (Iwatsuki et al., 2005; Sun et al., 2001).

CBF and AP-1 are known to cooperate in the transactivation of the metalloproteinase MMP-13 (Selvamurugan et al., 1998; Porte et al., 1999; Hess et al., 2001). MMP-13 is an interstitial collagenase able to degrade native fibrillar collagens in the triple helical domain in vivo that is required for endochondral bone formation and homeostasis (Inada et al., 2004; Stickens et al., 2004). Recent evidence points to a critical and specific function of MMP-13 derived from activated stromal cells and inflammation-responsive hematopoietic cells at sites of tumor tissue (Egeblad and Werb, 2002; Mueller and Fusenig, 2004) and in the chick chorioallantoic membrane in response to angiogenic factors (Seandel et al., 2001; Zijlstra et al., 2004). We provide experimental evidence that loss of EC-intrinsic MMP-13 expression caused by *junB* ablation and, consequently, impaired CBFβ expression results in diminished collagenolytic activity of JunB-deficient ECs and failure in sprouting and tube formation. Accordingly, *mmp-13* −/− ECs also exhibited strongly reduced tube formation on Matrigel, suggesting that loss of MMP-13 may account for the angiogenic defects in JunB-deficient ECs. Reexpression of CBFβ in JunB-deficient cells led them to regain MMP-13 expression and tube formation. Thus, our data provide strong evidence for a regulatory JunB–CBFβ–protease axis in the EC sprouting process. Interestingly, *mmp-13* knockout mice display delayed enchondral ossification and reduced vessel ingrowth into the primary ossification center (Inada et al., 2004; Stickens et al., 2004), presumably caused by the reduced bioavailability of VEGF. It was concluded that MMP-13 produced by chondrocytes might be critical for the release of matrix-bound VEGF. So far there exists only one study stressing an EC-intrinsic role for MMP-13 as an important effector of nitric oxide-activated EC migration (Lopez-Rivera et al., 2005). Thus, our findings underscore the importance of MMP-13 in EC function, which may also contribute to the phenotype of MMP-13–deficient mice.

In conclusion, we demonstrate an essential cell-autonomous function of JunB in ECs and identify CBFβ as a novel JunB target. The fact that a common target of CBF and AP-1, MMP-13, is crucial for capillary-like tube formation suggests important tasks for CBFβ in diseased neovascularization such as cancer and retinopathy. Henceforth, it will be interesting to dissect not only the individual contribution of autocrine and paracrine pathways addressed by JunB but also JunB/CBFβ converging on commonly known, as well as yet to be defined, targets. It is conceivable that these pathways may prove to be a promising target for antiangiogenic therapy in the future.

Materials and methods

Transgenic mice

The generation of *junB* +/− (Schorpp-Kistner et al., 1999), *junB* flox (Kenner et al., 2004), *Tie-2*-Cre (Constien et al., 2001), *Collagen1α2*-Cre (Florin et al., 2004a, 2006), and *mmp13* −/− mice (Stickens et al., 2004) has been previously described. *Tie-2*-lacZ (Schlaeger et al., 1997) transgenic mice were provided by U. Deutsch (University of Berne, Berne, Switzerland). The *Tie-2*-Cre or *Collagen1α2*-Cre mice were crossed to *junB* +/− mice and their offspring were mated to *junB* flox/flox mice to obtain *junB* −/Δ mice. *junB* +/flox, *junB* +/Δ, *junB* −/flox, or *junB* +/+ mice were used as controls. For genotyping, genomic DNA was isolated and PCR was performed for the *junB* locus as previously described (Schorpp-Kistner et al., 1999). Embryos were fixed and stained for LacZ activity, as previously described (Licht et al., 2004). For image acquisition, a dissecting microscope (M 10; Leica) equipped with a PlanApo 1.0×/0.04 NA objective (Leica) and a digital camera (DXM1200; Nikon) were used. Images were processed with Photoshop CS software (Adobe).

All mice used in this study were housed in specific pathogen-free and light-, temperature- (21°C), and humidity-controlled (50–60% relative humidity) conditions. Food and water were available ad libitum. The procedures for performing animal experiments were in accordance with the principles and guidelines of the Arbeitsgemeinschaft der Tierschutzbeauftragten in Baden-Württemberg (officials for animal welfare) and were approved by the Regierungspräsidium Karlsruhe.

Cell culture and luciferase reporter gene assay

END cells were established by infection of ECs derived from midgestation embryos with the N-TKmT retrovirus, as previously described (Reiss et al., 1998). END cells expressed endothelial marker genes (VE-cadherin, CD31, CD105, and VEGFR-2), as determined by immunofluorescence staining or FACS analysis, and were able to endocytose DiI-acetyl-LDL particles (CellSystems). For hypoxia treatment, END cells were placed in an incubator with 1.5% O_2 partial pressure (CB; Binder) for 16 h.

The murine CBFβ promoter (nt −1,496 to −251) was amplified by PCR using the primers CBFβ1 and CBFβ2 (Table S1, available at http://www.jcb.org/cgi/content/full/jcb.200605149). The promoter was ligated to a tata-luciferase reporter plasmid (van Dam et al., 1998). F9 teratocarcinoma cells were cultured and transiently transfected as previously described (Hess et al., 2001). 1 μg CBFβ promoter fused to the luciferase reporter gene was cotransfected with 0.5 μg AP-1 expression plasmids (JunB, c-Fos, and ATF-2 under control of the Rous sarcoma virus promoter) and 0.05 μg *renilla*-luciferase for normalization. Cells were lysed and luciferase activity was determined using the Dual-Luciferase reporter system (Promega) and a Sirius luminometer (Berthold).

Isolation of primary ECs

Microvascular ECs were isolated from mouse lungs using a magnetic cell separation method, as previously described (Dong et al., 1997). In brief, magnetic beads (Dynabeads; Dynal) were coated with anti-CD31 antibodies (Mec13.3; BD Biosciences). Two mouse lungs of similar genotype were pooled, minced, and digested with collagenase A solution (Roche). Cells were incubated with anti-CD31–coated Dynabeads and separated in a magnetic field. After washing away unbound cells, the beads were released by trypsin/EDTA treatment. Isolated ECs were analyzed for the expression of endothelial marker genes as described in Cell culture and luciferase reporter gene assay.

Mouse aortic ring assay

Aortic explants were prepared as previously described (Zhu and Nicosia, 2002). Mouse aortae were dissected free from connective tissue, cut in 1–2-mm pieces using a scalpel, and washed in ice-cold DME. For each tissue explant, a drop of 40 μl rat type I collagen (Serva) was placed into a culture dish. Aortic rings were placed into the droplet with fine forceps. After polymerization of the gel, the dishes were filled with culture medium (see Isolation of primary ECs) supplemented with 40 or 100 ng/ml recombinant VEGF-A164 (R&D Systems). Capillary sprouting was quantified in a semiquantitative manner by classification of aortic rings from 1 (no capillary sprouting) to 4 (strong outgrowth reaching the margins of the collagen matrix). In each experiment, at least nine aortic rings of control and *junB* $-/\Delta^{Coll}$ mice were scored, and the experiment was repeated four times.

In vitro angiogenesis and invasion assay

Matrigel (BD Biosciences) was mixed with an equal volume ice-cold DME. 150 μl Matrigel solution was poured into 48-well plates and incubated for at least 6 h at 37°C. 3.5×10^4 cells were seeded on top of the gel and incubated for 6–24 h. Capillary-like tube formation was quantified by counting interendothelial spaces in three randomly chosen optical fields. Each assay was performed in triplicate.

For analysis of invasive capacity, ECs were seeded on a type I collagen gel and grown to confluency. After incubation for 10 d, the invasion of EC into the underlying collagen gel was assessed by microscopic observation of different focus planes. For image acquisition, an inverse light microscope (DMIL; Leica) equipped with Plan Apo objectives (4×/0.1 NA and 10×/0.2 NA) and a DXM1200 digital camera were used. Images were processed with Photoshop CS software.

BrdU incorporation
Proliferation was assessed by BrdU incorporation and subsequent FACS analysis using the BrdU Flow kit (BD Biosciences) according to the instructions of the manufacturer. In brief, 10^5 ECs were seeded on 6-well plates and cultured for 24 h. Cells were incubated with medium containing BrdU for 2 h and subjected to the assay protocol.

Lateral migration assay
ECs were plated in 6-well dishes and grown to confluency. The monolayer was wounded by scratching with a pipette tip and photographed. After 24 and 48 h, the wounded area was photographed again and the wound closure was measured using ImageJ software (National Institutes of Health).

Retroviral gene transfer
JunB or CBFβ coding sequences were amplified by PCR using the primers junB1, junB2, CBFβ3, and CBFβ4 (Table S1). The fragments were inserted into the pMXpie vector. JunB-deficient END cells were transduced with retroviral vectors as previously described (Cerwenka et al., 2000). In brief, cellular supernatant containing viral particles was transferred to 8×10^4 END cells in 24-well plates. Cells were transduced by spin infection (3 h; 2,000 rpm) and thereafter cultured in selective media containing 3 μg/ml puromycin (Sigma-Aldrich). Efficiency of retroviral infection was determined by FACS analysis of GFP reporter gene expression.

cDNA microarray analysis
Total RNA was extracted from END cells cultured under normoxic or hypoxic conditions (1.5% O_2 for 16 h) using TRIZOL reagent as suggested by the manufacturer (Invitrogen). A collection of 15,247 sequences from embryonic cDNA libraries was used to generate the 15K NIA cDNA microarray. Details on probe labeling, hybridization, data acquisition, and analysis were previously described (Florin et al., 2004b).

RT-PCR analysis
Total RNA was isolated from mouse tissue or cultured ECs using peqGold RNApure reagent (PEQLAB) according to the instructions of the manufacturer. RNA was reverse transcribed using AMV reverse transcriptase (Promega). cDNA was used for semiquantitative RT-PCR or quantitative real-time RT-PCR using Absolute QPCR SYBR Green mix (ABgene) and a thermal cycler (iCycler; BioRad Laboratories) controlled by MyiQ software (BioRad Laboratories). Primer sequences for MMPs were previously described (Martinez et al., 2005). For primer sequences for β-tubulin, HPRT, CBFβ5 and -6, and JunB 3 and 4 see Table S1.

Western blot analysis
Whole-cell extracts or nuclear extracts were prepared as previously described (Andrecht et al., 2002). Proteins were separated by SDS-PAGE and transferred to nitrocellulose membrane. Immunodetection was performed using an enhanced chemiluminescence system (Perkin Elmer Life Science) and the following primary antibodies: anti-JunB (1:500; N17; Santa Cruz Biotechnology, Inc.), anti-RCC1 (1:500; BD Biosciences), anti-CBFβ (1:500; E20; Santa Cruz Biotechnology, Inc.), and anti-HSC70 (1:10,000; Noventa).

Collagenase activity assay
Collagenolytic activity in supernatants of EC cultures was determined using the Collagenase Activity Assay kit (CHEMICON International, Inc.) according to the instructions of the manufacturer. Equal numbers of control and JunB-deficient cells were seeded and cultured for 24–48 h. 100 μl of the supernatant were then subjected to the assay protocol.

Immunofluorescence staining
Cryosections were fixed with acetone at −20°C and stained at RT, as previously described (Hartenstein et al., 2006). An epifluorescence microscope (DMLB; Leica) equipped with PlanApo objectives (10×/0.4 NA, 20×/0.7 NA, 40×/0.85 NA, and 63× oil/1.3 NA) was used. A DXM1200 digital camera was used for documentation, and images were processed with Photoshop CS software. The primary antibodies used were CD31 (BD Biosciences), JunB (210; Santa Cruz Biotechnology, Inc.), and CBFβ (E20; Santa Cruz Biotechnology, Inc.). The secondary antibodies used were goat anti–rat–Alexa Fluor 488 (Invitrogen) and goat anti–rabbit–Cy3 (Dianova).

ChIP Assay
A ChIP kit (Millipore) was used according to the instructions of the manufacturer. The antibodies used (all from Santa Cruz Biotechnology, Inc.) were JunB (c11), ATF-2 (c19), Fra-1 (N17), and c-Fos (4). For primer sequences for the amplification of the CBFβ promoter see Table S1.

In brief, 2.5×10^6 END cells were incubated with 200 μM $CoCl_2$ for 4 h. Cells were cross-linked in 1% formaldehyde for 20 min at RT. Cells were washed and sonicated using a Bioruptor device (Diagenode). Immunoprecipitation was performed using protein A–Agarose. After washing, protein–DNA complexes were eluted and cross-links were reversed. Proteins were digested by proteinase K and DNA was extracted using QIAquick spin columns (QIAGEN).

Statistical analysis
The SD is indicated by error bars. Unpaired two-tailed *t* tests were performed using Sigma Plot 8.0 software. Significance was assumed for P values ($P < 0.05$; indicated by asterisks).

Online supplemental material
Table S1 shows details on PCR primer sequences. Fig. S1 shows the investigation of placental development, Fig. S2 shows the microscopic evaluation of aortic ring assays, Fig. S3 shows the validation of retroviral gene transfer, and Fig. S4 shows *mmp-13* promoter analysis in ECs.

The authors thank U. Deutsch and A. Cerwenka for providing transgenic mice and retroviral vectors, respectively, M. Hahn for advice on DNA microarrays, M. Sator-Schmitt, B. Vonderstrass, and S. Teurich for technical assistance, and J. Hess for providing *mmp-13* reporter constructs and CBF expression plasmids and critically reading the manuscript.

This work was supported by the Deutsche Forschungsgemeinschaft (AN 182/8-2 and Transregio SFB23; B. Arnold, P. Angel, and M. Schorpp-Kistner) and the Bundesministerium für Bildung und Forschung (NGFN2: SMP RNA 01GR0418, BTN 01GS0460 to P. Lichter)

Submitted: 23 May 2006
Accepted: 31 October 2006

References

Andrecht, S., A. Kolbus, B. Hartenstein, P. Angel, and M. Schorpp-Kistner. 2002. Cell cycle promoting activity of JunB through cyclin A activation. *J. Biol. Chem.* 277:35961–35968.

Angel, P., and M. Karin. 1991. The role of Jun, Fos and the AP-1 complex in cell-proliferation and transformation. *Biochim. Biophys. Acta*. 1072:129–157.

Bergman, M.R., S. Cheng, N. Honbo, L. Piacentini, J.S. Karliner, and D.H. Lovett. 2003. A functional activating protein 1 (AP-1) site regulates matrix metalloproteinase 2 (MMP-2) transcription by cardiac cells through interactions with JunB-Fra1 and JunB-FosB heterodimers. *Biochem. J.* 369:485–496.

Blyth, K., E.R. Cameron, and J.C. Neil. 2005. The RUNX genes: gain or loss of function in cancer. *Nat. Rev. Cancer*. 5:376–387.

Carmeliet, P. 2000. Mechanisms of angiogenesis and arteriogenesis. *Nat. Med.* 6:389–395.

Cerwenka, A., A.B. Bakker, T. McClanahan, J. Wagner, J. Wu, J.H. Phillips, and L.L. Lanier. 2000. Retinoic acid early inducible genes define a ligand family for the activating NKG2D receptor in mice. *Immunity*. 12:721–727.

Constien, R., A. Forde, B. Liliensiek, H.J. Grone, P. Nawroth, G. Hammerling, and B. Arnold. 2001. Characterization of a novel EGFP reporter mouse to monitor Cre recombination as demonstrated by a Tie2 Cre mouse line. *Genesis*. 30:36–44.

Coultas, L., K. Chawengsaksophak, and J. Rossant. 2005. Endothelial cells and VEGF in vascular development. *Nature*. 438:937–945.

Davis, G.E., and D.R. Senger. 2005. Endothelial extracellular matrix: biosynthesis, remodeling, and functions during vascular morphogenesis and neovessel stabilization. *Circ. Res.* 97:1093–1107.

Dong, Q.G., S. Bernasconi, S. Lostaglio, R.W. De Calmanovici, I. Martin-Padura, F. Breviario, C. Garlanda, S. Ramponi, A. Mantovani, and

A. Vecchi. 1997. A general strategy for isolation of endothelial cells from murine tissues. Characterization of two endothelial cell lines from the murine lung and subcutaneous sponge implants. *Arterioscler. Thromb. Vasc. Biol.* 17:1599–1604.

Eferl, R., and E.F. Wagner. 2003. AP-1: a double-edged sword in tumorigenesis. *Nat. Rev. Cancer*. 3:859–868.

Egeblad, M., and Z. Werb. 2002. New functions for the matrix metalloproteinases in cancer progression. *Nat. Rev. Cancer*. 2:161–174.

Florin, L., H. Alter, H.J. Grone, A. Szabowski, G. Schutz, and P. Angel. 2004a. Cre recombinase-mediated gene targeting of mesenchymal cells. *Genesis*. 38:139–144.

Florin, L., L. Hummerich, B.T. Dittrich, F. Kokocinski, G. Wrobel, S. Gack, M. Schorpp-Kistner, S. Werner, M. Hahn, P. Lichter, et al. 2004b. Identification of novel AP-1 target genes in fibroblasts regulated during cutaneous wound healing. *Oncogene*. 23:7005–7017.

Florin, L., J. Knebel, P. Zigrino, B. Vonderstrass, C. Mauch, M. Schorpp-Kistner, A. Szabowski, and P. Angel. 2006. Delayed wound healing and epidermal hyperproliferation in mice lacking JunB in the skin. *J. Invest. Dermatol.* 126:902–911.

Gerald, D., E. Berra, Y.M. Frapart, D.A. Chan, A.J. Giaccia, D. Mansuy, J. Pouyssegur, M. Yaniv, and F. Mechta-Grigoriou. 2004. JunD reduces tumor angiogenesis by protecting cells from oxidative stress. *Cell*. 118:781–794.

Hartenstein, B., S. Teurich, J. Hess, J. Schenkel, M. Schorpp-Kistner, and P. Angel. 2002. Th2 cell-specific cytokine expression and allergen-induced airway inflammation depend on JunB. *EMBO J.* 21:6321–6329.

Hartenstein, B., B.T. Dittrich, D. Stickens, B. Heyer, T.H. Vu, S. Teurich, M. Schorpp-Kistner, Z. Werb, and P. Angel. 2006. Epidermal development and wound healing in matrix metalloproteinase 13-deficient mice. *J. Invest. Dermatol.* 126:486–496.

Hess, J., D. Porte, C. Munz, and P. Angel. 2001. AP-1 and Cbfa/runt physically interact and regulate parathyroid hormone-dependent MMP13 expression in osteoblasts through a new osteoblast-specific element 2/AP-1 composite element. *J. Biol. Chem.* 276:20029–20038.

Hess, J., B. Hartenstein, S. Teurich, D. Schmidt, M. Schorpp-Kistner, and P. Angel. 2003. Defective endochondral ossification in mice with strongly compromised expression of JunB. *J. Cell Sci.* 116:4587–4596.

Hess, J., P. Angel, and M. Schorpp-Kistner. 2004. AP-1 subunits: quarrel and harmony among siblings. *J. Cell Sci.* 117:5965–5973.

Hoang, M.V., M.C. Whelan, and D.R. Senger. 2004. Rho activity critically and selectively regulates endothelial cell organization during angiogenesis. *Proc. Natl. Acad. Sci. USA*. 101:1874–1879.

Inada, M., Y. Wang, M.H. Byrne, M.U. Rahman, C. Miyaura, C. Lopez-Otin, and S.M. Krane. 2004. Critical roles for collagenase-3 (Mmp13) in development of growth plate cartilage and in endochondral ossification. *Proc. Natl. Acad. Sci. USA*. 101:17192–17197.

Iwatsuki, K., K. Tanaka, T. Kaneko, R. Kazama, S. Okamoto, Y. Nakayama, Y. Ito, M. Satake, S. Takahashi, A. Miyajima, et al. 2005. Runx1 promotes angiogenesis by downregulation of insulin-like growth factor-binding protein-3. *Oncogene*. 24:1129–1137.

Jain, R.K. 2003. Molecular regulation of vessel maturation. *Nat. Med.* 9:685–693.

Kenner, L., A. Hoebertz, T. Beil, N. Keon, F. Karreth, R. Eferl, H. Scheuch, A. Szremska, M. Amling, M. Schorpp-Kistner, et al. 2004. Mice lacking JunB are osteopenic due to cell-autonomous osteoblast and osteoclast defects. *J. Cell Biol.* 164:613–623.

Licht, A.H., S. Raab, U. Hofmann, and G. Breier. 2004. Endothelium-specific Cre recombinase activity in flk-1-Cre transgenic mice. *Dev. Dyn.* 229:312–318.

Liu, Y., and D.R. Senger. 2004. Matrix-specific activation of Src and Rho initiates capillary morphogenesis of endothelial cells. *FASEB J.* 18:457–468.

Lopez-Rivera, E., T.R. Lizarbe, M. Martinez-Moreno, J.M. Lopez-Novoa, A. Rodriguez-Barbero, J. Rodrigo, A.P. Fernandez, A. Alvarez-Barrientos, S. Lamas, and C. Zaragoza. 2005. Matrix metalloproteinase 13 mediates nitric oxide activation of endothelial cell migration. *Proc. Natl. Acad. Sci. USA*. 102:3685–3690.

Martinez, C., S. Bhattacharya, T. Freeman, M. Churchman, and M. Ilyas. 2005. Expression profiling of murine intestinal adenomas reveals early deregulation of multiple matrix metalloproteinase (Mmp) genes. *J. Pathol.* 206:100–110.

Mokry, J., D. Cizkova, S. Filip, J. Ehrmann, J. Osterreicher, Z. Kolar, and D. English. 2004. Nestin expression by newly formed human blood vessels. *Stem Cells Dev*. 13:658–664.

Mueller, M.M., and N.E. Fusenig. 2004. Friends or foes - bipolar effects of the tumour stroma in cancer. *Nat. Rev. Cancer*. 4:839–849.

Namba, K., M. Abe, S. Saito, M. Satake, T. Ohmoto, T. Watanabe, and Y. Sato. 2000. Indispensable role of the transcription factor PEBP2/CBF in angiogenic activity of a murine endothelial cell MSS31. *Oncogene*. 19:106–114.

Nausch, N., L. Florin, B. Hartenstein, P. Angel, M. Schorpp-Kistner, and A. Cerwenka. 2006. Cutting edge: the AP-1 subunit JunB determines NK cell-mediated target cell killing by regulation of the NKG2D-ligand RAE-1epsilon. *J. Immunol.* 176:7–11.

Oettgen, P. 2001. Transcriptional regulation of vascular development. *Circ. Res.* 89:380–388.

Parekh, V., A. McEwen, V. Barbour, Y. Takahashi, J.E. Rehg, S.M. Jane, and J.M. Cunningham. 2004. Defective extraembryonic angiogenesis in mice lacking LBP-1a, a member of the grainyhead family of transcription factors. *Mol. Cell. Biol.* 24:7113–7129.

Passegue, E., W. Jochum, M. Schorpp-Kistner, U. Mohle-Steinlein, and E.F. Wagner. 2001. Chronic myeloid leukemia with increased granulocyte progenitors in mice lacking junB expression in the myeloid lineage. *Cell*. 104:21–32.

Peck, J.W., M. Oberst, K.B. Bouker, E. Bowden, and P.D. Burbelo. 2002. The RhoA-binding protein, rhophilin-2, regulates actin cytoskeleton organization. *J. Biol. Chem.* 277:43924–43932.

Pepper, M.S. 2001. Role of the matrix metalloproteinase and plasminogen activator-plasmin systems in angiogenesis. *Arterioscler. Thromb. Vasc. Biol.* 21:1104–1117.

Porte, D., J. Tuckermann, M. Becker, B. Baumann, S. Teurich, T. Higgins, M.J. Owen, M. Schorpp-Kistner, and P. Angel. 1999. Both AP-1 and Cbfa1-like factors are required for the induction of interstitial collagenase by parathyroid hormone. *Oncogene*. 18:667–678.

Reiss, Y., G. Hoch, U. Deutsch, and B. Engelhardt. 1998. T cell interaction with ICAM-1-deficient endothelium in vitro: essential role for ICAM-1 and ICAM-2 in transendothelial migration of T cells. *Eur. J. Immunol.* 28:3086–3099.

Risau, W. 1997. Mechanisms of angiogenesis. *Nature*. 386:671–674.

Schlaeger, T.M., S. Bartunkova, J.A. Lawitts, G. Teichmann, W. Risau, U. Deutsch, and T.N. Sato. 1997. Uniform vascular-endothelial-cell-specific gene expression in both embryonic and adult transgenic mice. *Proc. Natl. Acad. Sci. USA*. 94:3058–3063.

Schorpp-Kistner, M., Z.Q. Wang, P. Angel, and E.F. Wagner. 1999. JunB is essential for mammalian placentation. *EMBO J.* 18:934–948.

Seandel, M., K. Noack-Kunnmann, D. Zhu, R.T. Aimes, and J.P. Quigley. 2001. Growth factor-induced angiogenesis in vivo requires specific cleavage of fibrillar type I collagen. *Blood*. 97:2323–2332.

Selvamurugan, N., W.Y. Chou, A.T. Pearman, M.R. Pulumati, and N.C. Partridge. 1998. Parathyroid hormone regulates the rat collagenase-3 promoter in osteoblastic cells through the cooperative interaction of the activator protein-1 site and the runt domain binding sequence. *J. Biol. Chem.* 273:10647–10657.

Speck, N.A., and D.G. Gilliland. 2002. Core-binding factors in haematopoiesis and leukaemia. *Nat. Rev. Cancer*. 2:502–513.

Stickens, D., D.J. Behonick, N. Ortega, B. Heyer, B. Hartenstein, Y. Yu, A.J. Fosang, M. Schorpp-Kistner, P. Angel, and Z. Werb. 2004. Altered endochondral bone development in matrix metalloproteinase 13-deficient mice. *Development*. 131:5883–5895.

Sun, L., M. Vitolo, and A. Passaniti. 2001. Runt-related gene 2 in endothelial cells: inducible expression and specific regulation of cell migration and invasion. *Cancer Res.* 61:4994–5001.

Takakura, N., T. Watanabe, S. Suenobu, Y. Yamada, T. Noda, Y. Ito, M. Satake, and T. Suda. 2000. A role for hematopoietic stem cells in promoting angiogenesis. *Cell*. 102:199–209.

van Dam, H., S. Huguier, K. Kooistra, J. Baguet, E. Vial, A.J. van der Eb, P. Herrlich, P. Angel, and M. Castellazzi. 1998. Autocrine growth and anchorage independence: two complementing Jun-controlled genetic programs of cellular transformation. *Genes Dev.* 12:1227–1239.

Wang, Q., T. Stacy, J.D. Miller, A.F. Lewis, T.L. Gu, X. Huang, J.H. Bushweller, J.C. Bories, F.W. Alt, G. Ryan, et al. 1996. The CBFbeta subunit is essential for CBFalpha2 (AML1) function in vivo. *Cell*. 87:697–708.

Zenz, R., R. Eferl, L. Kenner, L. Florin, L. Hummerich, D. Mehic, H. Scheuch, P. Angel, E. Tschachler, and E.F. Wagner. 2005. Psoriasis-like skin disease and arthritis caused by inducible epidermal deletion of Jun proteins. *Nature*. 437:369–375.

Zhang, G., C.R. Dass, E. Sumithran, N. Di Girolamo, L.Q. Sun, and L.M. Khachigian. 2004. Effect of deoxyribozymes targeting c-Jun on solid tumor growth and angiogenesis in rodents. *J. Natl. Cancer Inst.* 96:683–696.

Zhu, W.H., and R.F. Nicosia. 2002. The thin prep rat aortic ring assay: a modified method for the characterization of angiogenesis in whole mounts. *Angiogenesis*. 5:81–86.

Zijlstra, A., R.T. Aimes, D. Zhu, K. Regazzoni, T. Kupriyanova, M. Seandel, E.I. Deryugina, and J.P. Quigley. 2004. Collagenolysis-dependent angiogenesis mediated by matrix metalloproteinase-13 (collagenase-3). *J. Biol. Chem.* 279:27633–27645.